Available online at www.sciencedirect.com
SCIENCE DIRECT®
International Journal of Solids and Structures 43 (2006) 1746–1763
INTERNATIONAL JOURNAL OF SOLIDS and STRUCTURES
www.elsevier.com/locate/ijsolstr

Performance of metallic honeycomb-core sandwich beams under shock loading

H.J. Rathbun [a], D.D. Radford [b], Z. Xue [c], M.Y. He [a], J. Yang [a], V. Deshpande [b], N.A. Fleck [b], J.W. Hutchinson [c], F.W. Zok [a,*], A.G. Evans [a]

[a] *Materials Department, University of California, Santa Barbara, CA 93106, USA*
[b] *Department of Engineering, University of Cambridge, Trumpington St., Cambridge CB2 1PZ, UK*
[c] *Division of Engineering and Applied Sciences, Harvard University, Cambridge, MA 02138, USA*

Received 1 December 2004; received in revised form 16 June 2005
Available online 26 August 2005

Abstract

Stainless steel square honeycomb core sandwich and solid monolithic beams have been subjected to high-pressure, short-duration impulses using a shock simulation technique involving high-speed impact of Al foam projectiles. The experiments have been designed to achieve two objectives: (i) to demonstrate the benefits of sandwich construction, and (ii) to assess the fidelity of dynamic finite element calculations in simulating the structural response. The results affirm that, when subjected to impulse levels representative of those associated with nearby explosions, the sandwich beams exhibit smaller displacements than the solid beams at equivalent weight. The benefit is especially large at lower impulses where the effective dynamic strength of the honeycomb core prevents crushing. The measurements and finite element simulations having greatest relevance to the shock resistance are found to correspond closely, particularly the displacements and the core crushing strains. One implication is that the dynamic finite element model has the requisite fidelity at impulse levels of interest.

Keywords: Shock loading; Sandwich beams; Dynamic simulations

1. Introduction

The deformations experienced by metallic structures subject to nearby explosions are of broad interest. The shock loadings in such circumstances are characterized by a sharp pressure spike (of order

* Corresponding author. Tel.: +1 805 893 8699; fax: +1 805 893 8486.
E-mail address: zok@engineering.ucsb.edu (F.W. Zok).

0020-7683/$ - see front matter © 2005 Elsevier Ltd. All rights reserved.
doi:10.1016/j.ijsolstr.2005.06.079

Nomenclature

d_c	core web thickness
d_f	face sheet thickness
E	Young's modulus
H_c	core height
I_{ref}	reference impulse
I	applied impulse
I_i	initial impulse
I_r	rebound impulse
ℓ_0	projectile length
L	half loading span
L_c	cell size
m	strain rate exponent
m_f	mass per unit area of solid material
M	mass per unit area
p_{ref}	reference pressure
t_{cr}	crushing time
t_s	bending/stretching response time
v_0	impact velocity
v_r	rebound velocity
w	final back face deflection
ε_d^{mf}	densification strain for metal foam
ε_p	effective plastic strain
$\dot{\varepsilon}_p$	effective plastic strain rate
$\dot{\varepsilon}_0$	reference strain rate
$\dot{\varepsilon}_y$	yield strain
η	normalized hydrodynamic pressure
γ	shear strain
$\bar{\rho}$	core relative density
ρ_f	density of solid material
ρ_{mf}	density of metal foam
σ_0	quasi-static flow stress
σ_c	applied compressive stress
σ_Y	yield stress of solid material
σ_y^{mf}	yield stress of metal foam
τ	impact duration time
τ_{ref}	reference duration time

10–100 MPa), followed by an exponential attenuation persisting for tens of micro-seconds (Smith and Hetherington, 1994; Ashby et al., 2000; Taylor, 1947).

Recent analyses of clamped beams and plates subject to spatially uniform impulses (Fleck and Deshpande, 2004; Qiu et al., 2003; Xue and Hutchinson, 2004) have provided the following insights and implications (Fig. 1).

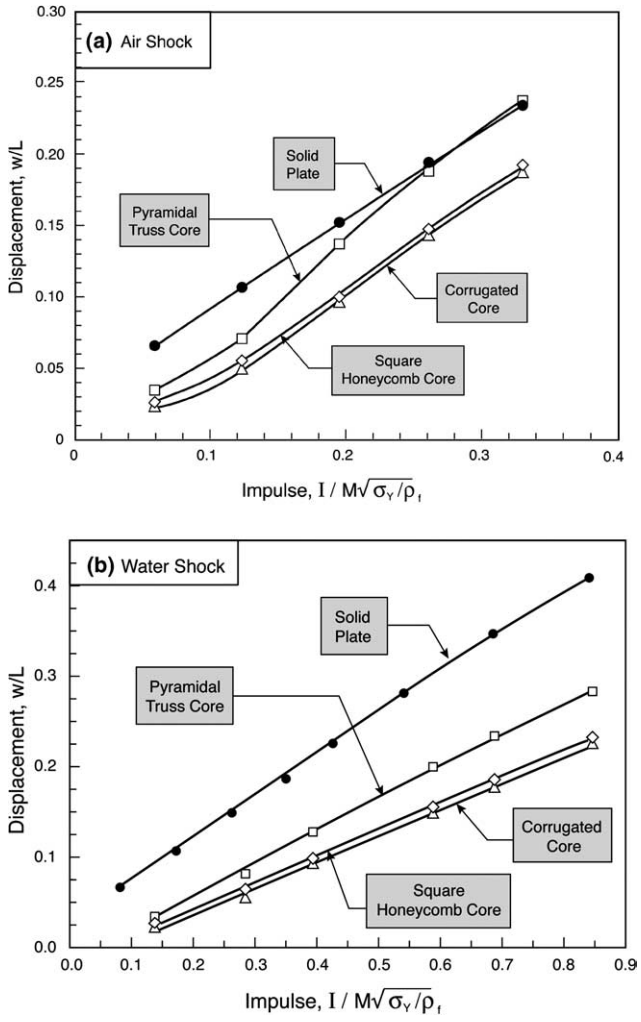

Fig. 1. Synopsis of deflection predictions for beams with various core types, subject to spatially uniform impulse (a) in air and (b) under water. Here, M is the mass per unit area of the beam.

(i) Metallic sandwich structures outperform monolithic solids of equivalent weight in the bend-dominated domain, i.e., when the deflections are small relative to the support span. The benefits diminish at large deflections, as the response becomes stretch-dominated.

(ii) The benefits of sandwich construction depend on core topology. Core designs that afford simultaneous crushing and stretching resistance are preferred. Desirable topologies include square honeycombs and corrugated plates.

(iii) Additional benefits of sandwich construction derive from fluid/structure interaction effects (Xue and Hutchinson, 2004; Fleck and Deshpande, 2004). This happens because the impulse imparted to a sandwich structure due to an underwater shock is lower than that imparted to a solid monolithic structure at the same mass. The ensuing advantages of sandwich designs can be substantial (Fig. 1(b)).

The focus of the present article is on validation of these analyses, as well as their extension to spatially more complex impulses, through a combination of experiments and simulations.

2. Objectives and approach

2.1. Shock simulation

Because of safety issues associated with detonation of explosive materials, a laboratory protocol that simulates impulses from shocks is required. One approach uses metal foam projectiles fired from a gas gun at high velocities (Fig. 2) (Radford et al., 2005). This procedure produces a "patch" loading over a narrow range relative to the support span.

The resulting pressures and duration times have been obtained from experiments and analyses of foam projectiles impacting a massive *elastic* target. In this case, the pressure at the impact site scales with a reference value, given by (Radford et al., 2005):

$$p_{\text{ref}} = \sigma_{\text{y}}^{\text{mf}} + \frac{\rho_{\text{mf}} v_0^2}{\varepsilon_{\text{d}}^{\text{mf}}} \tag{1}$$

where v_0 is the impact velocity, and $\sigma_{\text{y}}^{\text{mf}}$, $\varepsilon_{\text{d}}^{\text{mf}}$ and ρ_{mf} are the yield strength, densification strain and density of the foam projectile, respectively. For a prescribed projectile material, the pressure is adjusted through v_0. The corresponding impulse duration scales with a reference time, given by (Radford et al., 2005):

$$\tau_{\text{ref}} = \frac{\ell_0 \varepsilon_{\text{d}}^{\text{mf}}}{v_0} \tag{2}$$

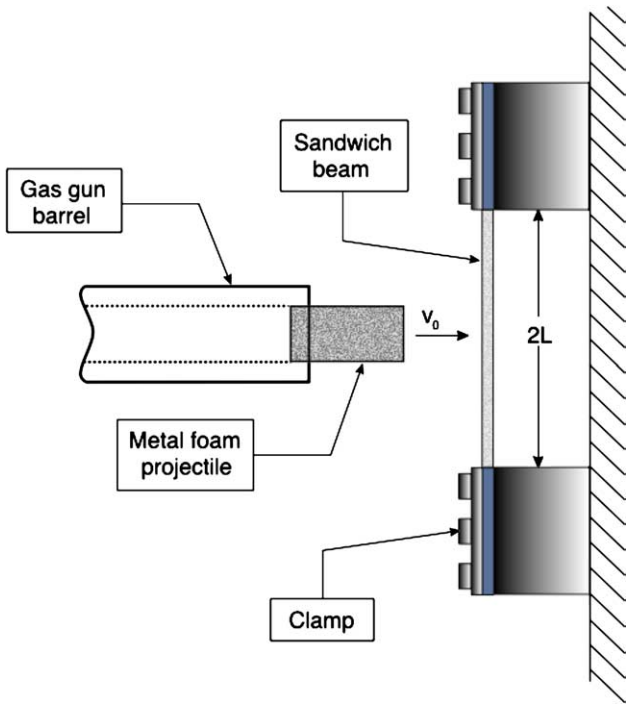

Fig. 2. A schematic showing the test used to impose an impulse representative of a blast.

where ℓ_0 is the projectile length. The consequent reference impulse per unit area is:

$$I_{\text{ref}} = p_{\text{ref}} \cdot \tau_{\text{ref}} \tag{3}$$

The actual values of the loading parameters (p, τ and I) depend on the mass ratio (projectile/target) and the ratio of quasi-static yield strength $\sigma_{\text{y}}^{\text{mf}}$ to the hydrodynamic pressure $\rho_{\text{mf}} v_0^2/\varepsilon_{\text{d}}^{\text{mf}}$ exerted by the projectile (Radford et al., 2005), characterized by

$$\eta = \frac{\sigma_{\text{y}}^{\text{mf}} \varepsilon_{\text{d}}^{\text{mf}}}{\rho_{\text{mf}} v_0^2} \tag{4}$$

In the limit where the mass ratio $\to 0$ and $\eta \to 0$, the pressure and duration reduce to the reference values ($p = p_{\text{ref}}$ and $\tau = \tau_{\text{ref}}$), and the applied impulse becomes:

$$I = I_{\text{ref}} = p_{\text{mf}} \ell_0 v_0 \tag{5}$$

The actual pressures and durations achieved in experiments on clamped beams differ somewhat, because of the finite compliance and yield strength of the target. For example, for sandwich beams, the pressure at the impact site is lower than that obtained with elastic targets, because of concomitant core crushing during application of the pressure pulse. Consequently, to present experimental results, it is preferable to use a measurable quantity, notably the nominal impulse, given by:

$$I = \rho_{\text{mf}} \ell_0 (v_0 + v_{\text{r}}) \tag{6}$$

where v_{r} is the rebound velocity (taken as a positive quantity). For the test conditions employed here, it will be shown that the rebound velocity is small in relation to the initial velocity ($v_{\text{r}}/v_0 < 0.05$), whereupon:

$$I \approx \rho_{\text{mf}} \ell_0 v_0 \tag{7}$$

Note that this impulse is the same as that for a projectile impacting a massive elastic target (5).

Through appropriate selection of the projectile properties and velocity, pressure pulses representative of actual explosions can be achieved. For illustration, selected results for TNT explosions (scaled accordingly) are plotted in Fig. 3. For blast scenarios of current interest (such as the specific example shown in the figure), the pressures and impulses fall roughly in the range 1–100 MPa and 1–10 kPa s, respectively. The lower end of each range corresponds to air blasts and the higher end to water blasts. As shown later, the values obtained in the present experiments fall within the targeted ranges; specifically, the pressures are about 10–100 MPa and the impulses are about 1–5 kPa s.

2.2. Structural response times

While metal foam impact is capable of realizing impulses with the requisite pressure/time profiles, problems in interpretation are encountered when scaled-down, laboratory-sized specimens are used. The difficulty relates to the two characteristic response times of the structure relative to pulse duration: one for core crushing and the other for bending/stretching. For sandwich beams, the characteristic core crushing time is given approximately by:

$$t_{\text{cr}} \approx \sqrt{\frac{H_{\text{c}} m_{\text{f}}}{p_{\text{ref}}}} \tag{8}$$

where m_{f} is the mass per unit area of the face sheet and H_{c} is the core height. The second is the time associated with beam bending and stretching (Qiu et al., 2003; Taylor, 1947):

$$t_{\text{s}} = L \sqrt{\frac{\rho_{\text{f}}}{\sigma_{\text{Y}}}} \tag{9}$$

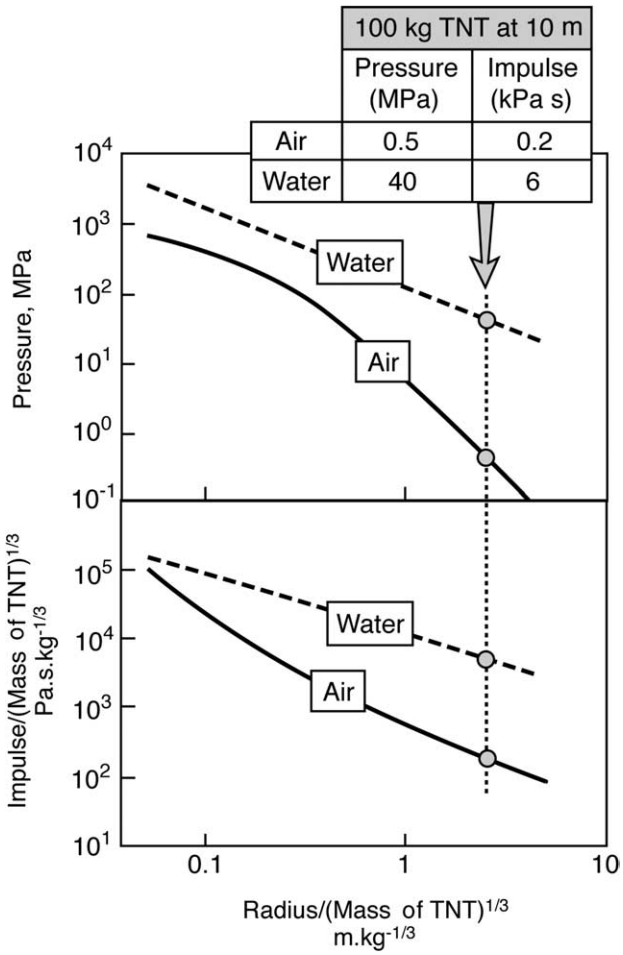

Fig. 3. Pressures and impulses delivered by underwater and air explosions as a function of the distance from the explosion, scaled accordingly (adapted from Ashby et al., 2000). One specific combination of TNT mass and distance from the target reveals typical (absolute) values of pressures and impulses.

where L is the half-span, and ρ_f and σ_Y are the mass density and yield strength of the face material. When $\tau_{ref} \ll t_{cr} \ll t_s$, the dynamic analysis can be simplified significantly because the three stages of the blast—application of impulse, core crushing and beam bending—can be de-coupled (Fleck and Deshpande, 2004). Otherwise, when τ_{ref} is of the order of t_{cr} or t_s, the interactions between the projectile and the beam must be taken into account explicitly. The present measurements and simulations reveal that, in the scaled-down specimens, the latter conditions prevail, precluding use of a de-coupled impulsive model to interpret the experimental results. Consequently, a fully coupled model based on finite element simulations is employed to describe the structural response of both the beam and the projectile.

2.3. Experiments

Despite some of its limitations, the metal foam method is envisaged as an effective technique for imposing front face velocities in a range relevant to shock scenarios. In the current investigation, the method is

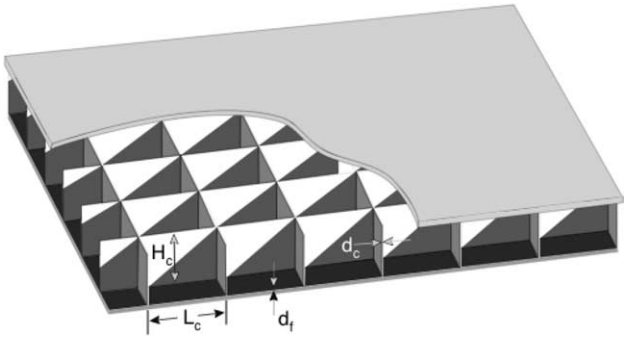

Fig. 4. Honeycomb-core sandwich geometry.

used to study the dynamic response of beams with square honeycomb cores (Fig. 4). Some quasi-static experiments are also performed, to demonstrate several consequences of the dynamics. The two primary objectives of the experimental program are:

(i) Demonstrate that a sandwich beam with a square honeycomb core exhibits a smaller deflection than an equivalent weight solid monolithic beam at prescribed impulse.
(ii) Provide experimental observations and measurements of beam deflections and core deformations that can be used for comparison with dynamic finite element simulations.

2.4. Simulations

Recently, constitutive laws for metallic sandwich cores subject to quasi-static loadings have been devised and validated by both experiment and fully meshed finite element calculations (Xue and Hutchinson, 2005; Zok et al., 2004). The development of analogous dynamic laws has proved more challenging, because of the strong influence of inertia on core crushing (Vaughn et al., 2005). In lieu of such models, in the present study, full 3-D simulations of the experiments are performed, incorporating all of the geometric aspects of the target and of the impacting foam. The finite element code ABAQUS Explicit is used for this purpose. The beam and projectile geometries duplicate those used in the experiments and the strain-rate sensitivities of the materials are included. The objective is to compare the simulations with the measurements in order to establish the fidelity of the numerical model under impulse loadings representative of actual shocks. An ensuing step, to be included in a later publication, will be the development of a dynamic constitutive law.

3. Experimental and simulation procedures

3.1. Beam design and manufacturing

Pertinent dimensions of the sandwich beams are summarized in Table 1. The corresponding equivalent weight solid was 1.6 mm thick. The sandwich design was based in part on concurrent studies of strength optimization of honeycomb core beams (Rathbun et al., 2004; Zok et al., in press). Additionally, consideration was given to the following constraints:

(i) Based on previous manufacturing experience, the web thickness was maintained above a critical value (about 0.2 mm). Otherwise, an excessive fraction of the steel is locally consumed during brazing, thereby compromising node integrity.

Table 1
Geometric parameters for honeycomb core sandwich beam

Core height, H_c	8.3 mm
Face sheet thickness, d_f	0.64 mm
Core cell size, L_c	12.7 mm
Core cell wall thickness, d_c	0.25 mm
Core relative density, $\bar{\rho}$	4%

(ii) To ensure beam behavior, the ratio of core thickness to loading span was maintained below 0.05 (Wicks and Hutchinson, 2001; Zok et al., 2003).
(iii) The test specimens were designed to ensure a minimum of two full core cells across the width. A related constraint was imposed by the projectile diameter (29.5 mm). An acceptable design was obtained by selecting a cell size, L_c, of 12.7 mm and a specimen width of 32 mm (yielding about 2.5 cells across the width). One unsatisfactory consequence is that the projectile diameter (29.5 mm) is slightly smaller than the beam width, causing the core response to vary across the width. To minimize the associated problems, the specimen was aligned to ensure that the impact site was centered where four neighboring square honeycomb cells intersect.

The beams were fabricated using 304 stainless steel for both the core and the face sheets. To produce the core, an array of steel slotted strips was assembled in a wine-box configuration (Cote et al., 2004; Zok et al., in press). The core members were then simultaneously brazed to both each other and the face sheets. This was accomplished by placing at the intersection points small amounts of the braze material: a mixture of Nicrobraz Cement 520 and Nicrobraz 31 braze powder, both supplied by Wal Colmonoy (Madison Heights, MI). The assembly of core members and face sheets was then heated in a vacuum furnace for 2 h at 1075 °C. To enable clamping of the specimen ends (Fig. 2), the cells between the clamps were filled with an epoxy over a distance of about 50 mm at each end.

3.2. Testing

The dynamic performance of both the sandwich and the solid beams was ascertained (Fig. 2). During testing, both beam ends were rigidly clamped over a length of about 50 mm. The loading span was 200 mm. The projectiles were machined from an aluminum alloy foam, trade name ALPORAS (Miyoshi et al., 2000), with relative density ~11% (Table 2). Their diameter was selected to match the barrel diameter (29.5 mm). To avert tumbling, the projectile length was slightly greater than the diameter ($\ell_0 = 32$ mm). The impulse was varied by changing the impact velocity, over the range 140–470 m/s. Impact velocities were measured using four laser diode velocity gates, located at the end of the barrel. The resulting reference pressures (Eq. (1)) are in the range 10–100 MPa and impulse durations (Eq. (2)) are 50–150 μs (Fig. 5). The consequent impulses are about 1–5 kPa s.

Table 2
Properties of Alporas Al alloy foam

Yield strength	3 MPa
Young's modulus	1 GPa
Densification strain	0.7
Density	300 kg/m^3
Elastic Poisson ratio	0.3
Plastic Poisson ratio	0

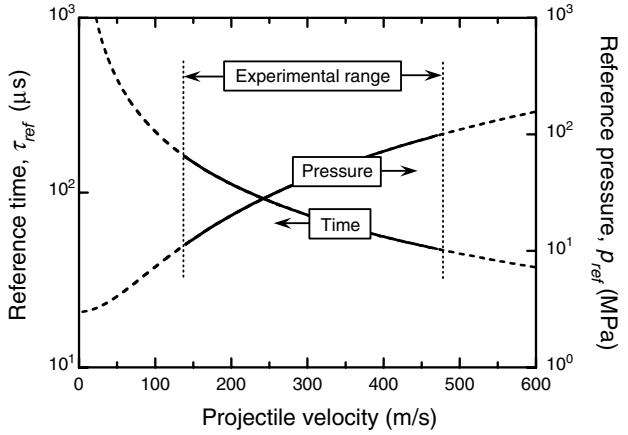

Fig. 5. Reference impulse parameters for the present experiments.

To observe the deformation during impact, high-speed photographic sequences were taken using a Hadland Imacon 790 image converter camera. Inter-frame times of 40 μs and exposure times of 8 μs were used. Following each experiment, front and back face deflections were measured along the center-line of the projectile trajectory using a pair of calipers. The measurement locations coincided with a node where two web members intersected. In turn, the difference of these deflections was used to calculate the average through-thickness crushing strain beneath the impact site. Shear strains in the honeycomb cores were obtained from the rotations of the cells. The sandwich beams were subsequently sectioned by electro-discharge machining along the beam mid-plane, transverse to their long axis. These sections revealed the deformation and buckling patterns of the longitudinal core members directly beneath the impact site.

For comparison with the crushing behavior observed in the dynamic tests, quasi-static compression tests were performed on square honeycomb core specimens, at a nominal strain rate of $10^{-4}\,s^{-1}$. Tests were interrupted at various levels of plastic strain and the specimens subsequently sectioned in order to ascertain the buckling modes.

3.3. Finite element calculations

Three-dimensional dynamic finite-element calculations were used to simulate the tests. The faces of the sandwich beam and projectile were both fully meshed using eight-node linear brick elements with reduced integration. Such elements are capable of accurately capturing the stresses and strains. Each face sheet was discretized with five layers of elements through the thickness. The honeycomb core members were meshed using four-node linear shell elements with finite membrane strains. Five section integration points with Simpson's integration rule were used in each shell element. These elements allow large rotations and finite membrane deformation, making them particularly well-suited for post-buckling analyses. Additional studies showed that the current meshing scheme yielded results with a numerical error in maximum deflection of less than 1%. Finally, the webs were clamped to the face sheets at their connections. The beams were assumed to be rigidly clamped at both ends. The computations were conducted by imposing the initial velocity, v_0, uniformly on the projectile.

Since the Al-alloy foam has minimal strain-rate dependence (Ashby et al., 2000), a rate-independent constitutive law (Deshpande and Fleck, 2000) was adopted for the projectile. This constitutive law is capable of accurately modeling the dynamic response of the projectile under distributed pressure load (Deshpande and Fleck, 2000). The properties are given in Table 2, supplemented by compressive stress–strain data from the

literature (Radford et al., 2005), with zero artificial viscosity. Simulations have been carried out both with and without strain-rate dependence for the 304 stainless steel. For the rate dependent version, the flow stress $\sigma_0(\varepsilon_p, \dot{\varepsilon}_p)$ was taken as:

$$\frac{\sigma_0(\varepsilon_p, \dot{\varepsilon}_p)}{\sigma_0(\varepsilon_p, 0)} = 1 + \left(\frac{\dot{\varepsilon}_p}{\dot{\varepsilon}_0}\right)^m \tag{10}$$

where ε_p is the effective plastic strain, $\dot{\varepsilon}_p$ is the effective plastic strain rate $\sigma_0(\varepsilon_p, 0)$ is the quasi-static flow stress, and $\dot{\varepsilon}_0$ and m are material parameters determined by experiment. Dynamic measurements on stainless steels are well represented using the values $\dot{\varepsilon}_0 = 4916\ s^{-1}$ and $m = 0.154$ (Nemat-Nasser et al., 2001; Stout and Follansbee, 1986). The corresponding quasi-static tensile response is characterized by an initial yield stress of 200 MPa, followed by nearly linear hardening, with a tangent modulus of 2 GPa (Zok et al., 2004).

To explore the effects of the projectile/beam contact, two sets of preliminary calculations were carried out: one taking the contact to be frictionless and the other assuming sticking friction. The calculations revealed that the maximum deflections of the back face sheet differed by less than 0.1%, even for these two extremes. The differences in the crushing strains of the projectiles was slightly greater: the ones obtained with sticking friction being closer to the experimentally measured values. For this reason, all ensuing calculations were performed using sticking friction.

Additional three-dimensional finite element calculations were performed of the quasi-static core crushing, subject to direct compression. The meshing schemes were the same as those used for the dynamic simulations.

4. Experimental and numerical results

4.1. Beam deflection and deformation modes

Optical images of representative sandwich specimens tested at various impulse levels are presented in Fig. 6. The characteristic features include: (i) intense zones of plasticity at the impact site accompanied by plastic buckling of the core members; (ii) bending and stretching of both the core and the face sheets; and (iii) shear straining of the core, as evidenced by rotations of the transverse core members relative to the face sheets. At the highest impulse, the core shear strains attain values up to $\gamma \approx 12°$.

Measurements of the final back face deflection, when plotted against the nominal impulse (Fig. 7), affirm that the sandwich beams outperform the solid monolithic beams. The benefits of sandwich construction are particularly evident at low impulse levels ($I < 3$ kPa s), wherein the beam deflections are only about 20–50% of those for the solid beams. At higher impulse levels ($I > 3$ kPa s), the benefits diminish: the deflections of the sandwich beams being about 80% of the solid beams.

The primary results of the finite element calculations are summarized in Figs. 6 and 7, where they are compared with the corresponding experimental measurements and observations. The simulations capture most of the details of the deformation patterns quite realistically, including shearing of the core and buckling of the lateral webs. Moreover, the center displacements deduced from the calculations, when superposed in Fig. 7, are remarkably similar to the measurements. The correspondence affirms that the benefits of sandwich construction are duplicated with high fidelity. Corresponding results obtained by neglecting the material rate-dependence over-predict the measured deflections, typically by about 20%.

The relative effect of projectile rebound, characterized by the ratio of rebound impulse, I_r, to initial impulse, I_i, is illustrated in Fig. 8. The rebound impulse is found to be a small fraction of the initial value and hence its contribution to the total impulse is similarly small. Neglecting this contribution yields an error of $<5\%$ over the entire range of test conditions.

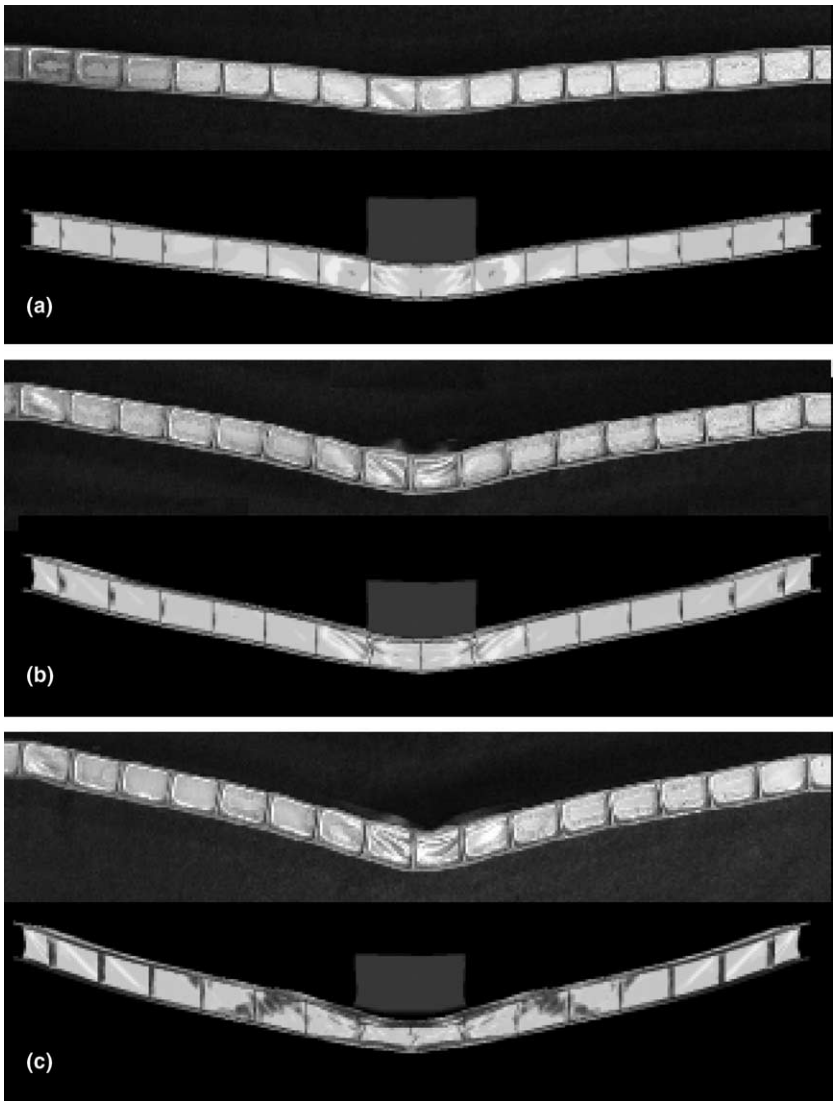

Fig. 6. Representative sandwich beams following dynamic testing, at impulse levels: (a) 2.7, (b) 3.8 and (c) 4.6 kPa s. The first image in each pair is a photograph of the actual test specimen; the second is from the finite element simulation.

4.2. Core crushing

The compressive strain experienced by the core at the center of the beam is plotted in Fig. 9. Significant core crushing only commences when $I > 3$ kPa s. It then rises rapidly with impulse, reaching about 0.5 at 4.6 kPa s. The onset of core crushing corresponds closely to the diminution in benefits (Fig. 7). The inference is that the advantages of the sandwich construction are greatest when the pressures are insufficient to cause significant core crushing: whereupon the high second moment of area (essential to high bending resistance) is retained.

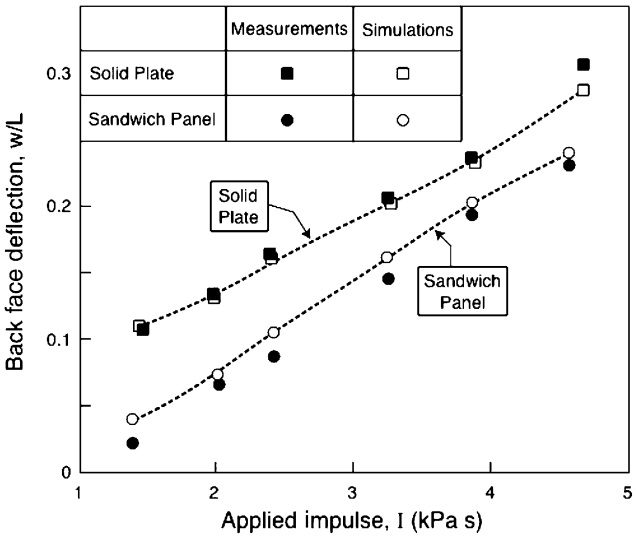

Fig. 7. Measurements and simulations of back face deflections as a function of applied impulse. The dotted lines are fits through the simulations.

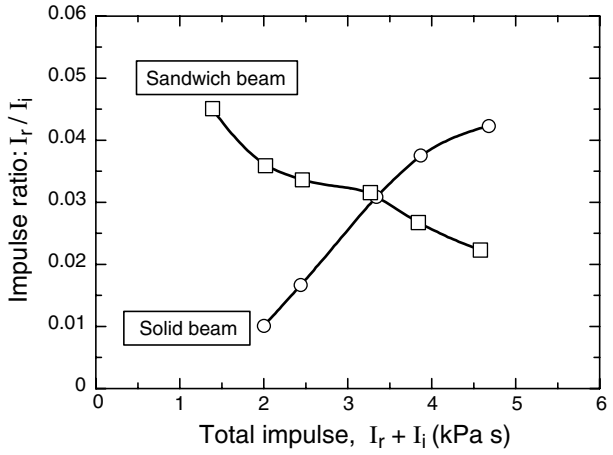

Fig. 8. Calculated rebound impulse for both sandwich and solid beams.

The effects of impulse on the mode of core crushing are illustrated in the transverse sections shown in Fig. 10. Beyond the critical impulse for crush initiation, all three longitudinal core members beneath the impact buckle plastically. The crushing strains are greatest in the central core member, because of the patch loading associated with the cylindrical projectiles. At the highest impulse, the central buckle is located within the upper segment of the core member, closest to the impact site, whereas the lower segment remains planar and largely undeformed. This pattern is reminiscent of that found when a metal rod is fired against a rigid surface (Abrahamson and Goodier, 1966). In some cases, the extensive bending of the buckled segment causes it to contact the upper face, while the associated plastic strain ruptures the node (Fig. 10(c)). A similar asymmetry from top to bottom is found in the two other longitudinal core members (at the

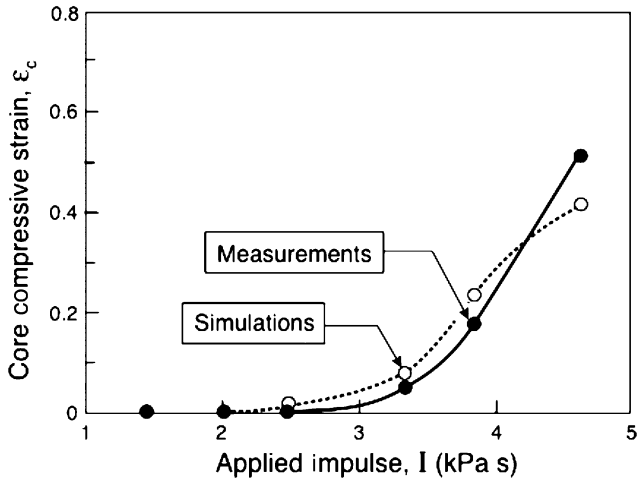

Fig. 9. Core compressive strain in sandwich beams at impact site.

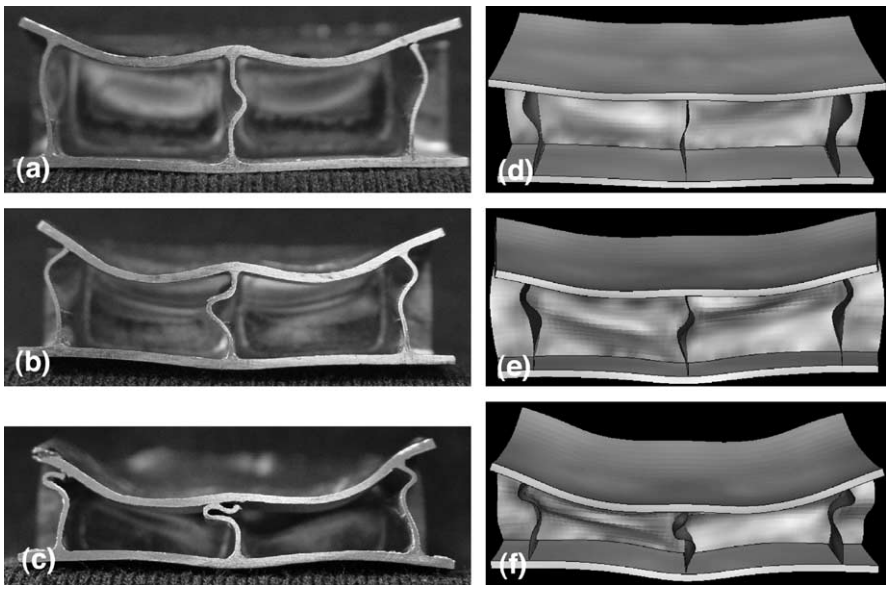

Fig. 10. Transverse cross-sections showing core crushing at impact sites, at impulse levels (a) 3.3, (b) 3.8 and (c) 4.6 kPa s. The sequence in (d)–(f) shows the corresponding finite element predictions at the same impulse levels.

periphery of projectile impact). In the latter cases, however, a lateral asymmetry arises from the non-uniformity in the displacement of the top face, causing the core members to buckle outward. Moreover, the axial strains are smaller. At lower impulse (3.3 kPa s), the central buckle is symmetric from top to bottom (Fig. 10(a)).

For comparison, the buckling response of the core under quasi-static loading is shown in Fig. 11. The two images correspond to the same crushing strains (0.16 and 0.47) experienced by the central core member at the two highest impulse levels (3.8 and 4.6 kPa s—Figs. 10(b) and (c)). Quasi-statically, the core members

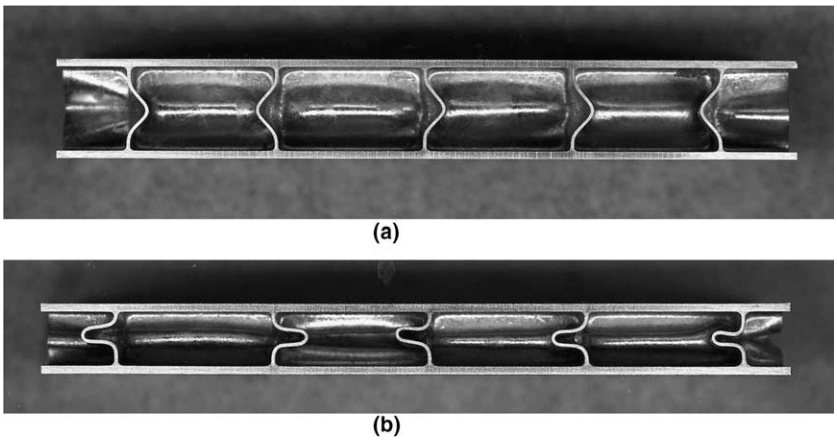

Fig. 11. Cross-sections through specimens tested in quasi-static compression at plastic strains of (a) 0.16 and (b) 0.47. Note the symmetry of each buckled core member.

always buckle symmetrically with respect to the two face sheets: some buckle to the right and others to the left. This response contrasts with the behavior at high impulse. The asymmetry is attributable to the stabilizing effects of core inertia on buckling (Vaughn et al., 2005).

The finite element calculations predict crushing response and buckling modes in broad agreement with the measurements. Specifically, the variation in crushing strain with impulse, plotted in Fig. 9, is adequately predicted. This is a particularly critical comparison because it requires the code to accurately capture the dynamic compressive stress–strain response of the core members. Additionally, the development of asymmetric buckling patterns at high impulse coincides with that seen experimentally (Fig. 10). Nevertheless, there are evident discrepancies, in the sense that the simulations reveal a buckling wavelength half that found experimentally. Although not clearly understood, it is surmised that the source of the discrepancy in buckling mode may be due to initial imperfection shapes not included in the numerical analysis. The excess braze present at the nodes may also play a role.

4.3. Assessment of time scales

Insights into the pertinent time scales associated with the pressure pulse as well as the deformation of the sandwich beams have been gleaned from a combination of experimental observations and numerical simulations. One set of observations is presented in Fig. 12. This shows a typical high-speed photographic sequence, obtained at an intermediate impulse. It illustrates two important features:

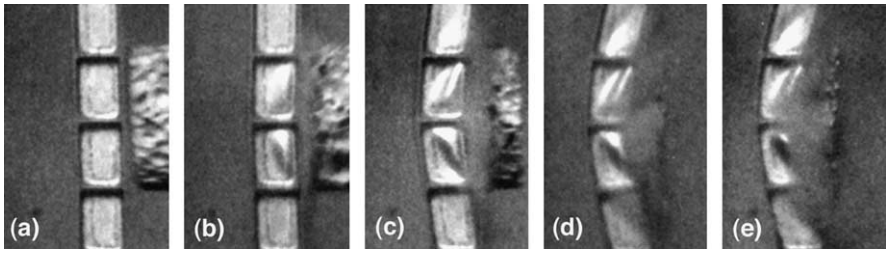

Fig. 12. A photographic sequence showing crushing of the foam projectile and deformation of the sandwich beam. The image in (a) was taken immediately before impact; the subsequent images were taken at 40 μs intervals. The impact velocity was 330 m/s.

(i) The foam projectile continues to densify in the two intervals between the first three frames (with 40 μs inter-frame time); densification appears to be complete during the third interval. The inference is that the impact duration falls in the range $\tau = 80$–120 μs. This duration is slightly larger than that expected when the same projectile impacts a rigid surface ($\tau_{ref} \approx 70$ μs) (Radford et al., 2005): a consequence of the finite compliance of the beam and its plastic deformation.

(ii) The evolution of the buckles, apparent on the external cell members near the center, demonstrates that core crushing has been completed within two inter-frame intervals after impact, in a time <80 μs. The implication is that the *impulse persists throughout the core-crushing phase*. This precludes use of a de-coupled shock model (Fleck and Deshpande, 2004), wherein the time scale of the pressure pulse is assumed to be small in relation to that for core crushing. The dynamics can only be captured through a fully coupled model for projectile and beam deformation, such as that employed in the present study.

Supporting evidence for these conclusions is obtained from the finite element calculations. Notably, for the highest impulse ($I = 4.6$ kPa s), the variation in pressure with time at the center of the impact area (Fig. 13) reveals that the projectile exerts pressure on the beam for about 120 μs, consistent with the time range inferred from the experimental observations. Additionally, the computed core compressive strain (Fig. 14) indicates that the time needed to complete core crushing is about 80 μs: again consistent with the observations. These numerical results independently verify that the pressure pulse persists over the duration of core crushing. They re-affirm the need for a fully coupled model to describe the structural response.

4.4. Dynamic core strength

To ascertain the degree of dynamic strengthening of the honeycomb cores under the current test conditions, comparisons have been made with simulations of the dynamic response of a similar square

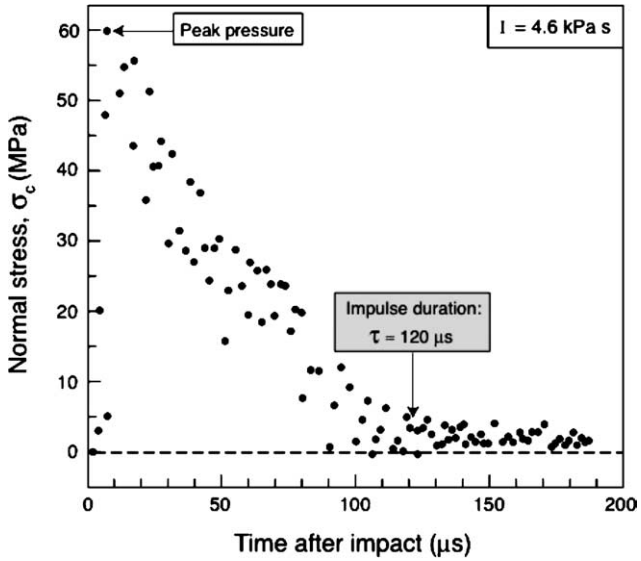

Fig. 13. Calculated variation in contact stress with time in the center element at the contact site at the highest impulse level. The impulse duration is estimated from the point at which the stress drops to a small fraction (<5%) of its peak value.

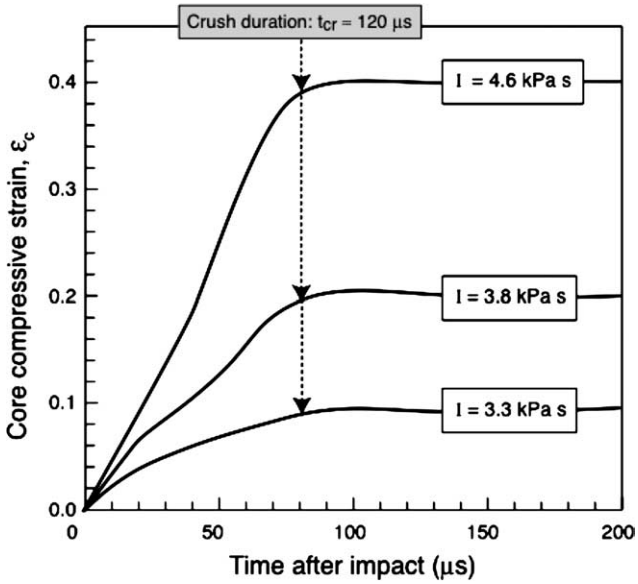

Fig. 14. Time-dependence of core crushing obtained from the calculations. Crushing is complete after about 120 μs, regardless of impulse level.

honeycomb core (Xue and Hutchinson, in press), conducted at constant front face velocity. The key results are plotted in Fig. 15, as a function of the normalized crushing velocity. Since the core crushing velocity in the beam tests is roughly constant at prescribed impulse (Fig. 14), this velocity can be superposed as a vertical line into Fig. 15 to assess the dynamic core strength. For the highest impulse, the dynamic core

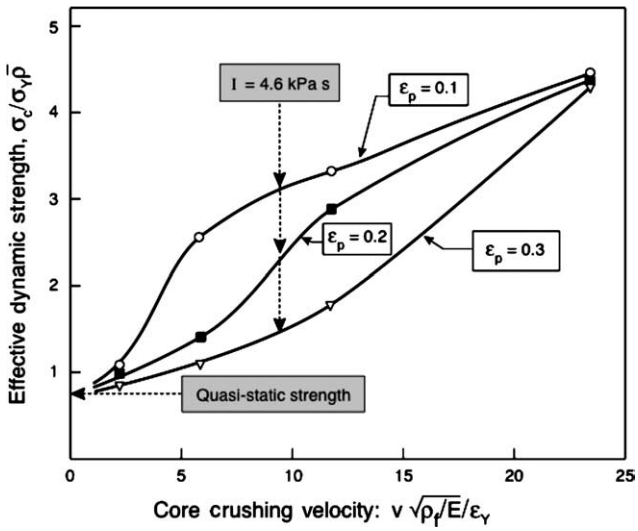

Fig. 15. Calculated effect of core crushing velocity on the effective dynamic strength. The velocity acquired at the highest impulse is superposed. Here $\bar{\rho}$, ρ_f, E and ε_y are the core relative density, the mass density of the solid material, the Young's modulus and the yield strain, respectively.

strength is about four times the quasi-static strength at small strains. Then, as crushing proceeds and the plastic strain increases, the effective strength decreases, ultimately reaching values of about twice the quasi-static strength before the crushing stops. The large effective strength during initial impact is the source of the especially high crushing resistance at smaller impulse levels.

5. Concluding remarks

The measurements and simulations affirm that, when subjected to impulses representative of those expected from nearby shocks, sandwich beams with square honeycomb cores exhibit appreciably smaller displacements than solid steel beams of equivalent mass. At lower impulses, where the core has sufficient dynamic strength to prevent appreciable crushing, the benefits of the sandwich structure are especially large.

From a shock simulation perspective, the major finding is that the measurements and calculations of the most important shock metrics correspond closely. These include the overall displacement of the beams and the crushing strain experienced by the core. The implication is that the dynamic code (ABAQUS Explicit) has the requisite fidelity at impulse levels of practical interest.

By combining input from measurements and simulations, it is found that, at the crushing velocities induced in the core, the effective dynamic strengths are larger than those determined quasi-statically (by a factor 2–4, depending on plastic strain). The major contribution to this strengthening is the transverse and axial inertia of the core (Vaughn et al., 2005).

Not all aspects of the simulations are in complete agreement with the experiments. Specifically, there is a discrepancy in the plastic buckling modes in the core. However, this discrepancy does not appear to adversely affect the quality of the simulations.

Acknowledgments

This work was supported by the ONR MURI program on Blast Resistant Structures through a sub-contract from Harvard University to the University of California at Santa Barbara (Contract No. 123163-03), US ONR IFO grant number N00014-03-1-0283 on The Science and Design of Blast Resistant Sandwich Structures and the Isaac Newton Trust, Trinity College Cambridge.

References

Abrahamson, G.R., Goodier, J.N., 1966. Dynamic flexural buckling of rods within an axial plastic compression wave. J. Appl. Mech., 241–247.

Ashby, M.F., Evans, A.G., Fleck, N.A., Gibson, L.J., Hutchinson, J.W., Wadley, H.N.G., 2000. Metal Foams: A Design Guide. Butterworth Heinemann.

Cote, F., Deshpande, V.S., Fleck, N.A., Evans, A.G., 2004. The out of plane compressive behavior of metallic honeycombs. Mater. Sci. Eng. A 380, 272–280.

Deshpande, V.S., Fleck, N.A., 2000. Isotropic constitutive models for metallic foams. J. Mech. Phys. Solids 48, 1253–1283.

Fleck, N.A., Deshpande, V.S., 2004. The resistance of clamped sandwich beams to shock loading. J. Appl. Mech. 71, 386–401.

Miyoshi, T., Itoh, M., Akiyama, S., Kitahara, A., 2000. ALPORAS Aluminum foam, production process, properties and applications. Adv. Eng. Mater. 2 (4), 179–183.

Nemat-Nasser, S., Guo, W.-G., Kihl, D.P., 2001. Thermomechanical response of AL-6XN stainless steel over a wide range of strain rates and temperatures. J. Mech. Phys. Solids 49, 1823–1846.

Qiu, X., Deshpande, V.S., Fleck, N.A., 2003. Finite element analysis of the dynamic response of clamped sandwich beams subject to shock loading. Euro. J. Mech. A/Solids 22, 801–814.

Radford, D.D., Deshpande, V.S., Fleck, N.A., 2005. The use of metal foam projectiles to simulate shock loading on a structure. Int. J. Impact Eng. 31, 1152–1171.

Rathbun, H.J., Wei, Z., He, M.Y., Zok, F.W., Evans, A.G., Sypeck, D.J., Wadley, H.N.G., 2004. Measurements and simulation of the performance of a lightweight metallic sandwich structure with a tetrahedral truss core. J. Appl. Mech. 71, 368–374.

Smith, P.D., Hetherington, J.G., 1994. Blast and Ballistic Loading of Structures. Butterworth Heinemann.

Stout, M.G., Follansbee, P.S., 1986. Strain rate sensitivity, strain hardening, and yield behavior of 304L stainless steel. Trans. ASME: J. Eng. Mater. Tech. 108, 344–353.

Taylor, G.I., 1947The Scientific Papers of G.I. Taylor (The Pressure and Impulse of Submarine Explosion Waves on Plates), vol. III. Cambridge University Press, Cambridge, UK, pp. 287–303.

Vaughn, D., Canning, M., Hutchinson, J.W., 2005. Coupled plastic wave propagation and column buckling. J. Appl. Mech. ASME 72 (1), 139–146.

Wicks, N., Hutchinson, J.W., 2001. Optimal truss plates. Int. J. Solids Struct. 38, 5165–5183.

Xue, Z., Hutchinson, J.W., 2004. A comparative study of impulse-resistant metal sandwich plates. Int. J. Impact Eng. 30, 1283–1305.

Xue, Z., Hutchinson, J.W., 2005. Constitutive model for quasi-static deformation of metallic sandwich cores. Int. J. Numer. Meth. Eng. 61 (13), 2205–2238.

Xue, Z., Hutchinson, J.W. Crush dynamics of square honeycomb sandwich cores. Int. J. Numer. Meth. Eng., in press.

Zok, F.W., Rathbun, H.J., Wei, Z., Evans, A.G., 2003. Design of metallic textile core sandwich panels. Int. J. Solids Struct. 40, 5707–5722.

Zok, F.W., Waltner, S.A., Wei, Z., Rathbun, H.J., McMeeking, R.M., Evans, A.G., 2004. A protocol for characterizing the structural performance of metallic sandwich panels: application to pyramidal truss cores. Int. J. Solids Struct. 41, 6249–6271.

Zok, F.W., Rathbun, H.J., He, M.Y., Ferri, E., Mercer, C., McMeeking, R.M., Evans, A.G. Structural performance of metallic sandwich panels with square honeycomb cores. Philos. Mag., in press.